FREE-MOE: TUNING-FREE MIXTURE-OF-EXPERTS PURIFYING LLMS TO THRIVE ACROSS ANY FIELD

Anonymous authors
Paper under double-blind review

ABSTRACT

The Mixture-of-Experts (MoE) framework efficiently scales large language models (LLMs) by selectively activating expert subnetworks, reducing computational costs. However, current MoE methods are costly in computation and include additional expert modules that require extra training data for tuning, leading to instability in the optimization process. To address these issues, we introduce FREE-MOE, a tuning-**free MoE** method that leverages pre-trained LLMs' inherent ability to generalize across a wide range of tasks and domains. FREE-MOE dynamically activates experts based on specific domains, achieves improvements while **1) requiring no extra model parameters and 2) being completely tuning-free.** Specifically, we design the DOWP Alg., a **D**omain-**O**riented **W**eight **P**urification Algorithm that purifies the weights in hidden layers and selects the optimal domain-specific experts of domain-specific experts in the hidden layers of the LLM to optimize activation decisions. The activated DSS-Experts, Domain-Specific Subnetwork Experts,can thereby concentrate on specialized task generation, outperforming the corresponding original model. Moreover, FREE-MOE incorporates a multi-level trainable router that activates only the most relevant subnetworks during task, effectively minimizing unnecessary inference computations. Comprehensive evaluations reveals that the DOWP Algorithm consistently achieves general performance gains of 2% to 3%, reaching up to 6.8% across datasets like MMLU, HumanEval, GSM8K, and etc. Additionally, when integrated into FREE-MOE framework, our method demonstrates a cumulative improvement of 1.11% in average. Findings indicate that FREE-MOE not only enhances overall computational efficiency but improves the model's adaptability across any field that encompassed in contemporary language generation model benchmarks, and can be seamlessly applied to any transformer-based LLMs. Code for this project will be released in reachable future.

1 INTRODUCTION

The demand for more powerful Large Language Models(LLMs) drives relentless expansion (Kaplan et al., 2020). Yet, the bigger the LLMs, the more they consume: computational resources, time, and energy, which in turn limits their scalability and application efficiency (Patterson et al., 2021; Strubell et al., 2019). Integrating the Mixture-of-Experts (MoE) framework with LLMs has emerged as a highly promising strategy for tackling these challenges, driving significant advancements in the field (Shazeer et al., 2017). Models like Switch Transformer and GShard have demonstrated that model capacity can be scaled to trillions of parameters without a proportional increase in computational costs during inference, setting new benchmarks in various natural language processing tasks (Fedus et al., 2022; Lepikhin et al., 2020). The key innovation of MoE lies in its use of sparse activation, where only a portion of the network is activated for any given input, allowing the model to possess greater capacity without a corresponding increase in computational demand (Zhou et al., 2022).

In a broader sense, the classical MoE approach operates by routing different inputs to specialized subnetwork experts within the model. These expert subnetworks are typically based on diverse foundational models, such as support vector machines (Collobert et al., 2002), Gaussian processes (Tresp, 2000), or hidden Markov models (Jordan & Jacobs, 1994), where the architecture enables the model to specialize in handling a wide range of tasks, improving its capacity to address complex and heterogeneous problem domains. Overall, the pioneering work on MoE introduced mechanisms

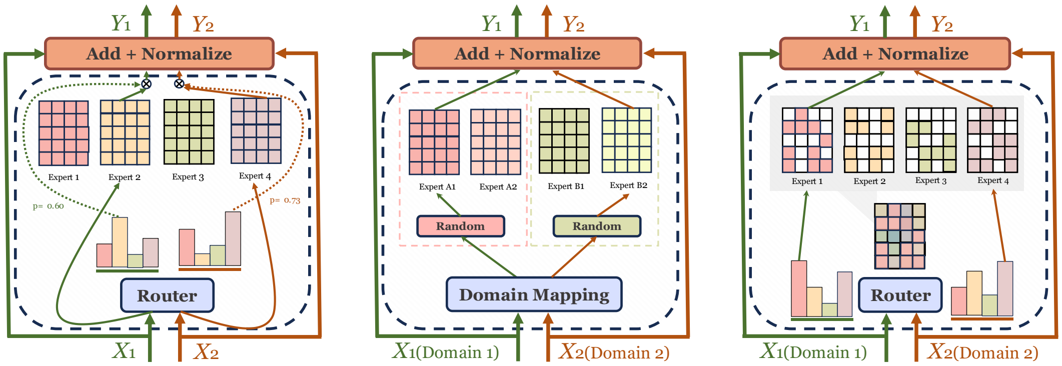

a) Sparse MoE (Top-1 Gating) **b) Domain Mapping + Random Gating** **c) Free-MoE**

Figure 1: The comparison between traditional MoE methods and our FREE-MOE. (a) represents Sparse MoE with top-1 gating, where the router activates only one expert per input based on the highest probability score. (b) shows the combination of grouped Domain Mapping and Random Gating MoE, which improves task-specific relevance but suffers from inefficiencies due to the random activation of experts. In contrast, (c) illustrates our FREE-MOE, which activates Domain-Specific Subnetwork Experts from pretrained LLMs using the Domain-Oriented Weight Purification Algorithm. FREE-MOE optimizes task-specific responses by purifying out domain-relevant weights to construct experts, achieving a tuning-free effect across diverse tasks.

for dynamically selecting experts, balancing computational load, and addressing challenges such as training instability and communication overhead in distributed systems.

Despite the tremendous potential of the MoE framework, its practical application continues to encounter several significant challenges. A key limitation is that maximizing the benefits of MoE typically requires large-scale, high-quality training data, especially in scenarios where data acquisition is costly or the quality of available data is inconsistent(Lepikhin et al., 2020). Previous work has focused on the field of non-trainable token-choice gating(Roller et al., 2021; Zuo et al., 2022; Gururangan et al., 2022; Ren et al., 2023; Kudugunta et al., 2021), exploring ways to achieve complete load balancing through specific gating mechanisms without requiring additional gating network parameters, thereby improving computational efficiency. However, stepping beyond this perspective, we need to reevaluate how to find more effective tuning-free methods within existing architectures to achieve a higher degree of tuning-free operation. Meanwhile, pre-trained LLMs, which have undergone large-scale training, possess strong capabilities to adapt to various tasks and may offer a new perspective. Therefore, we pose the following question:

Is it possible to leverage the subnetwork structures within the hidden layers of pre-trained LLMs to enhance task-specific performance and optimize the allocation of computational resources?

Through deeper investigation, we find that LLMs inherently function as implicit expert networks—while LLMs do not explicitly employ an MoE framework, the subnetworks activated by their hidden layers exhibit specialized behavior across different tasks and inputs. This enables pre-trained LLMs to adapt seamlessly to diverse tasks in tuning-free condition, particularly, without the need for external experts or the addition of significant new parameters. All that is required is an adaptive activation mechanism based on weight purification.

Building on this insight, we propose FREE-MOE, a novel tuning-free mixture of experts architecture designed to leverage the existing subnetwork expert mechanisms within pre-trained LLMs. The key principle of FREE-MOE is its self-directed purification process, where it identifies the input domain and selectively **purifies** the subnetwork weights, retaining only those relevant to the specific task. This allows FREE-MOE to adaptively activate only the expert subnetworks most pertinent to the given task. Compared to Sparse MoE and Domain-Mapping & Random Gating MoE architectures, FREE-MOE achieves improved efficiency and task-specific accuracy without increasing model complexity, thereby significantly reducing the computational burden typically associated with large models, as shown in Figure 1.

Specifically, purification represents the core solution for integrating the MoE framework into LLMs without additional tuning. This process leverages impurity removal and filtration mechanisms, applied during purification, to perform domain-driven expert selection. The core concept involves purifying the hidden layer weights by identifying domain-relevant features from the input, retaining high-contributing expert weights while filtering out irrelevant ones. This approach fully exploits the parameter sharing and hierarchical latent feature structures of pre-trained LLMs, achieving efficient utilization without tuning. In contrast to the simplistic expert selection strategies in Sparse MoE (Fedus et al., 2022) or the full expert activation of Dense MoE (Wu et al., 2022; Dua et al., 2022), purification significantly enhances both the accuracy and effectiveness of expert selection, optimizing model performance for task-specific contexts. Additionally, we define domain-specific expert derived from the hidden layers after purification, explicitly revealing the latent expertise within the pre-trained LLM subnetworks and enabling optimized task-oriented configurations. Compared to the auxiliary load-balancing loss mechanisms in ST-MoE(Zoph et al., 2022), these domain-specific experts offer superior adaptability, facilitating more efficient resource allocation for specialized tasks and substantially improving task-specific model performance. Lastly, we introduce a Trainable Router that dynamically monitors task requirements and domain characteristics, enabling real-time domain identification and efficient allocation of computational resources. Unlike the static mappings employed in Domain Mapping & Random Gating MoE (Ren et al., 2023), our method employs a more granular and dynamic domain activation strategy. This not only enhances operational efficiency but also leads to notable improvements in real-world task performance.

In this work, we present several key innovations that position FREE-MOE as a novel approach to leveraging LLMs within the MoE framework, addressing critical challenges in computational efficiency and task-specific performance:

- **Innovative MoE Architecture FREE-MOE**: FREE-MOE utilizes the latent subnetwork structures within pre-trained LLMs, eliminating the dependency of traditional MoE on large-scale, high-quality training data, and enabling adaptation to multi-task requirements without the need for fine-tuning.
- **Purification Mechanism on Weights**: This mechanism dynamically selects and activates subnetwork weights relevant to specific tasks, significantly improving the accuracy of expert selection. By purifying the hidden layer weights in pre-trained LLMs, the domain expertise of its subnetworks is made explicit.
- **A Multi-Level Trainable Dynamic Router**: We introduce a novel trainable router capable of real-time monitoring of task requirements and domain characteristics, dynamically identifying domains and efficiently allocating computational resources, particularly demonstrating significant advantages in multi-task scenarios.
- **Achieved Significant Performance Improvements Across Multiple Datasets**: Our approach achieved performance gains of 2% to 3% on datasets such as MMLU, MBPP, and GSM8K. Integrated into the FREE-MOE architecture, cumulative improvements of 1.11% validate the effectiveness and practicality of the method.

2 RELATED WORKS

2.1 THE MIXTURE OF EXPERTS

The Mixture of Experts (MoE) introduces multiple specialized expert networks, selectively activating a subset of experts during each inference to maintain model capacity while significantly reducing computational costs (Jacobs et al., 1991; Jordan & Jacobs, 1994; Chen et al., 1999; Tresp, 2000; Rasmussen & Ghahramani, 2001). MoE has demonstrated substantial potential in scaling model size and enhancing performance. Sparse gating MoE layers strike an effective balance between computational cost and model capacity by selecting only a small number of experts for computation per input (Shazeer et al., 2017; Riquelme et al., 2021). The GShard framework by Lepikhin et al. (2020) successfully trained ultra-large-scale models using conditional computation and automatic sharding techniques. Following this, Fedus et al. (2022) introduced the Switch Transformer, which further enhances training and inference efficiency through a simplified expert routing mechanism. To improve expert selection strategies, Zhou et al. (2022) proposed Expert Choice Routing, which optimizes expert selection and load balancing to enhance model performance and resource utilization.

In the realm of multi-task learning, Ma et al. (2018) developed the Multi-Gated Mixture-of-Experts (MMoE) model, which implements task-specific gating mechanisms to capture inter-task relationships. The commonality across MoE methods lies in leveraging sparse activation and expert selection to achieve a trade-off between model capacity and computational efficiency.

2.2 Interpretability of LLMs Mechanism

Interpretability of LLMs Mechanism represents a pivotal subfield within the broader study of LLM interpretability, focusing on uncovering the internal mechanisms of language models (Anthropic, 2023; Bricken et al., 2023). The dominant approach conceptualizes LLMs as "circuits", examining neural network hidden representations through feature visualization techniques. This approach has led researchers to identify larger functional components and uncover three key phenomena: Branch Specializatio, Weight Hierarchization and Equivariance (Voss et al., 2021; Petrov et al., 2021; Olah et al., 2020). Recent research has increasingly shifted towards single-layer and multi-layer attention models. In single-layer attention models, structures such as binary tables and skip-trigram tables can be derived from the model's weights. In multi-layer Transformer models, the concept of "induction heads" has emerged—modules formed by the combination of attention heads from different layers, designed to learn patterns within context (Elhage et al., 2021). The core of this research lies in treating neural network components as circuit-like functional modules, while emphasizing that the "circuits" within LLMs are not static but exhibit a high degree of dynamism and adaptability.

3 Method

3.1 Domain-Oriented Weight Purification

The Domain-Oriented Weight Purification, as shown in Figure 2, compresses matrix patches from hidden layers and ranks them by importance. Less relevant patches are purified, reducing complexity while preserving critical weights. This process forms the DSS-Expert for optimized task execution.

Clustering-based Classification. Consider multiple datasets $D_A, D_B, \ldots, D_n$, where each dataset corresponds to a distinct domain. These datasets are collectively aggregated to form a comprehensive main knowledge domain set, denoted as $\mathcal{D} = \{D_A, D_B, \ldots, D_n\}$, where each D_i corresponds to a specific domain that encapsulates specialized knowledge relevant to the given tasks. For a given task $\mathcal{T}$, the algorithm identifies the most suitable main knowledge domain D_j by computing the posterior probability $P(\mathcal{D} \mid \mathcal{T})$, which quantifies the likelihood of the task $\mathcal{T}$ belonging to each main domain $\mathcal{D}$. This selection process is expressed as:

$$D_j = \arg\max_{\mathcal{D}} P(\mathcal{D} \mid \mathcal{T}). \tag{1}$$

This ensures that the main domain D_j with the highest probability is chosen, aligning the task $\mathcal{T}$ with the most appropriate domain for further processing. Upon selecting the main knowledge domain D_j, the next step involves subdividing this domain into finer subdomains using K-means clustering. For each dataset in D_j, feature representations are extracted via the Transformer's embedding layer. The resulting set of feature vectors is denoted as $\mathcal{F}_j = \{F_{j_1}, F_{j_2}, \ldots, F_{j_m}\}$, where each F_{j_i} represents the feature vector corresponding to a data point in D_j. The K-means clustering algorithm is then applied to partition the feature set $\mathcal{F}_j$ into k distinct subdomains.

The clustering process aims to minimize the intra-cluster variance, measured by the Euclidean distance between each feature vector and its respective centroid. This optimization is formalized as follows:

$$\begin{aligned} S^* &= \arg\min_S \sum_{i=1}^{k} \sum_{F \in D_{j_i}} \left\| F - \frac{1}{|D_{j_i}|} \sum_{F \in D_{j_i}} F \right\|_2 \\ &= \arg\min_S \sum_{i=1}^{k} \sum_{F \in D_{j_i}} \| F - \mu_i \|_2. \end{aligned} \tag{2}$$

By minimizing this objective, the main knowledge domain D_j is effectively partitioned into a set of subdomains, each with a distinct centroid that captures the local structure of the domain. For any

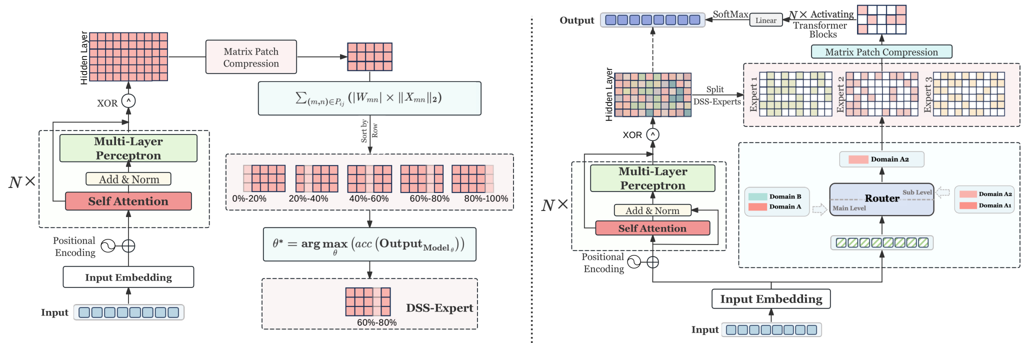

Step 1. Domain Oriented Weight Purification (1 layer)   Step 2. Free-MoE Structure Architecture

Figure 2: Two-step pipeline for our approach. *Step 1* demonstrates the DOWP (Domain Oriented Weight Purification) mechanism, where hidden layers extracted are compressed, sorted for domain-specific relevance via Equation 4, and further purifying MLP or Self-Attention Layers via Equation 6 to identify and retain the most relevant expert weights. *Step 2* illustrates the FREE-MOE pipeline, in which the router classifies the input by domain, assigning it to its DSS-Expert split from hidden layers, and the output are generated from the activated expert as the task-specific result.

new task $\mathcal{T}$, its feature representation $F_{\mathcal{T}} = Embedding(\mathcal{T})$ is extracted using the Transformer's embedding layer. The task is then assigned to the most relevant subdomain by calculating the Euclidean distance between F_T and the centroid μ_k of each subdomain. The subdomain that minimizes this distance is selected as follows:

$$k = \arg\min_{k} \|F_{\mathcal{T}} - \mu_k\|_2. \tag{3}$$

Once the subdomain D_{j_k} is identified, the task T will be assigned to this subdomain. Subsequently, task will be further distributed based on the characteristics of the subdomain, ensuring that the task's features align with the knowledge of the subdomain.

Metric Calculation on Patches. After identifying the subdomain D_{j_k}, this section is to quantify the critical information contained within it. Activation values serve as an effective metric for assessing the importance of neurons and connections within the network because they directly measure how strongly neurons respond to input features, reflecting their contribution to the network's output (Han et al., 2015). To perform this assessment, we begin by scaling the weight matrix W and feature matrix X. A scaling factor α reduces the dimensionality of the matrices, yielding a smaller matrix of size $\beta X \times \beta Y$ (where $\beta = 1/\alpha$). Each element in this reduced matrix corresponds to a patch P_{ij}, which represents a subregion of the original matrix and contains condensed information.

In passing, The scaling process ensures that there is no significant loss of information due to the Transformer's self-attention mechanism, which captures global dependencies across the entire input, facilitating information flow between and within patches (see Appendix A).

Afterwards, to further evaluate the significance of each patch, we calculate the following importance metric $\mathcal{M}_{ij}$:

$$\mathcal{M}_{ij} = \sum_{(m,n)\in P_{ij}} \left(|W_{mn}| \times \|X_{mn}\|_2\right). \tag{4}$$

This metric aggregates the weighted contributions of each element within the patch, thereby quantifying its relative importance to the overall network. The use of both weights and activation values ensures that the local information within each patch is preserved while facilitating efficient global interactions through the self-attention mechanism.

DSS-Experts Formation. After calculating the importance metrics $\mathcal{M}_{ij}$ for all patches, these patches are sorted in ascending order based on their importance scores: $\mathcal{M}_{(1)} \leq \mathcal{M}_{(2)} \leq \cdots \leq \mathcal{M}_{(k)}$, where $\mathcal{M}_{(i)}$ denotes the sorted importance scores, and k represents the total number of patches. This sorting process helps identify the least important patches for purification. A threshold range θ_r is then defined to govern the purification process, specifying the range of importance scores for the patches to be purified:

$$\theta_r = \{\mathcal{M}_{(i)} \mid \mathcal{M}_{(i)} \in [\theta_{\min}, \theta_{\max}]\}. \tag{5}$$

Here, θ_{min} and θ_{max} represent the lower and upper bounds of the importance scores targeted for purification. Patches within this range are considered less crucial to the model's overall performance and are therefore purified to reduce complexity while maintaining accuracy.

Following the purification process, the model's accuracy is re-evaluated to ensure minimal impact on performance. This accuracy, denoted as $\texttt{acc}(\theta_r)$, serves to validate the effectiveness of the purification. Subsequently, the outputs from each hidden layer are aggregated, incorporating the purified information to form the DSS-Expert. This approach allows the DSS-Expert to dynamically adapt to domain-specific tasks, ensuring optimized performance.

The final step involves optimizing the purification threshold. By iterating through various threshold ranges θ_r, the model's accuracy is assessed for each range, and the optimal threshold θ^* is identified:

$$\theta^* = \arg\max_{\theta_r} \left(\texttt{acc}(\texttt{Output}_{\text{MODEL}_{-\theta_r}}) \right). \tag{6}$$

This selection of θ^* ensures the model maintains maximum accuracy while eliminating the least significant patches, resulting in a highly efficient and accurate DSS-Expert, where $\mathcal{E}_{\text{DSS}} = \text{MODEL}_{-\theta^*}$.

Algorithm 1 Pytorch-style pseudocode for DOWP Algorithm.

```
# D_k: domain-specific data
# theta_init: initial threshold
# theta_max: maximum threshold
# delta_theta: step size

def optimize_threshold(D_k, Perf, theta_init, theta_max, delta_theta):
   # Initialize variables
   theta = theta_init
   best_perf = 0
   theta_k_star = theta_init

   # Step 1: Extract features and perform clustering
   F_k = embedding(D_k)
   subdomains = kmeans_clustering(F_k, k)

   while theta <= theta_max:
      # Step 2: Calculate importance and select patches for purification
      importance_scores = calculate_importance(subdomains, theta)
      selected_patches = [i for i in range(len(importance_scores))
                          if importance_scores[i] >= theta]

      # Step 3: Purify and evaluate model
      purified_model = purify_model(selected_patches)
      current_perf = Perf(purified_model, D_k)

      # Update best performance and optimal threshold
      if current_perf > best_perf:
         best_perf = current_perf
         theta_k_star = theta

      theta += delta_theta

   return theta_k_star
```

`Perf`: function to evaluate model performance on domain-specific data D_k.

3.2 FREE-MOE ARCHITECTURE

The FREE-MOE Architecture, illustrated in Figure 2, utilizes a multi-level trainable router to dynamically classify tasks into main knowledge domains and then subdomains. This routing mechanism activates the most relevant DSS-Experts, ensuring efficient and precise task processing by leveraging purified weights and task-specific parameters.

A Multi-level Trainable Router. We introduce a multi-level trainable router that classifies tasks through two hierarchical stages. First, the task embedding $F_{\mathcal{T}}$ is classified into a main knowledge domain D_j. Then, in the second stage, the task is further classified into a subdomain D_{j_k} within the selected main domain, as shown:

$$D_{j_k} = \mathcal{R}_{\text{sub},j}(\mathcal{R}_{\text{main}}(F_{\mathcal{T}})). \tag{7}$$

Here, $\mathcal{R}_{\text{main}}(F_{\mathcal{T}})$ maps the task embedding to a specific main domain D_j, and $\mathcal{R}_{\text{sub},j}(F_{\mathcal{T}})$, conditioned on this domain, further assigns the task to a subdomain D_{j_k}.

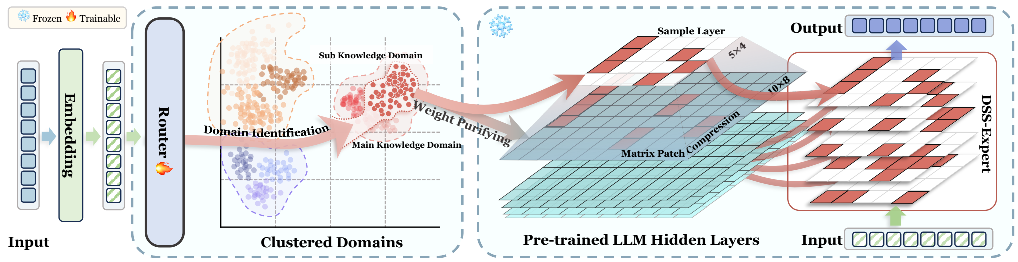

Figure 3: The inference flow through our FREE-MOE. The *input tokens* ( ) is first embedded and processed by a trainable ( ) router, where it is initially classified into the main knowledge domain and further into a sub knowledge domain. The *embedded input tokens* ( ) is then passed to the aggregated DSS-Expert, which are dynamically formed from the hidden layers of a frozen ( ) pre-trained LLM based on the identified domain, then *output tokens* ( ) are processed by the chosen expert to generate the task-specific result.

The router is trained by minimizing cross-entropy loss at both levels, optimizing the classification process:

$$\mathcal{L}_{\mathcal{R}} = \texttt{CrossEntropyLoss}(X) = -\sum_{k=1}^{m} y_k \log\left(P(D \mid X)\right), \tag{8}$$

where y_k is the true label for domain D, and $P(D \mid X)$ represents the predicted probability of the input X being classified into domain D.

The multi-level trainable router classifies tasks hierarchically into main and subdomains. The classification process is optimized using cross-entropy loss at both levels, enhancing precision across domains.

FREE-MOE Inference. The inference process in FREE-MOE begins with the input tokens X, which are first passed through an embedding layer into the embedded representation $\hat{X}$. The embedded tokens $\hat{X}$ are then fed into the router, a trainable classifier designed to assign the input to the most relevant domain. The router $\mathcal{R}$ classifies the input into a main knowledge domain and then sub knowledge domain, depending on the characteristics of the task, expressed as:

$$D_{m_i} = \mathcal{R}(\hat{X}). \tag{9}$$

After classification, the model proceeds DOWP. This step filters out irrelevant weights from the pre-trained LLM, retaining only those necessary for the selected domain. The purified weights, denoted as W_{purified}, form the core of the DSS-Expert:

$$W_{\text{purified}} = \texttt{DOWP}(W_{\text{pre-trained}}, D_{m_i}). \tag{10}$$

These purified expert in dynamically activated to process the embedded input $\hat{X}$, ensuring that only the domain-relevant parameters are used for the current task. The embedded input $\hat{X}$ is then forwarded through the selected DSS-Expert, which generate the intermediate output $\hat{Y}$. Finally, the intermediate output $\hat{Y}$ is subjected to a linear transformation and a softmax operation to produce the final output Y, which represents the model's prediction for the given task. Whole inference procedure is shown in Figure 2. By dynamically activating only the most relevant experts and focusing on task-specific weights, FREE-MOE optimizes both accuracy and computational efficiency. The process streamlines inference by adapting to the task, ensuring precise and efficient predictions without unnecessary computational overhead.

4 EXPERIMENTS

In this section, we evaluate the performance of our DOWP, FREE-MOE, comparing our approach with conventional baseline methods that rely on full network activation, as shown in Figure 4. Our DOWP algorithm consistently boosts performance across datasets: MMLU, MBPP, HumanEval, GSM8K and MathQA. When incorporated into the FREE-MOE architecture, it further improves efficiency, adaptability and stability.

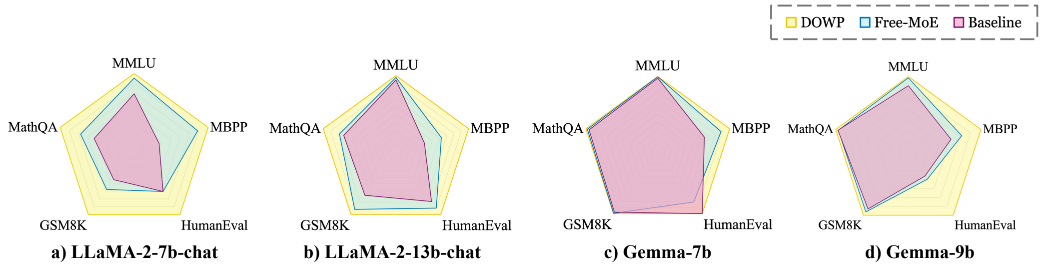

Figure 4: Performance comparison of different models applying DOWP and FREE-MOE. The radar charts illustrate the improvements across five datasets among DOWP , FREE-MOE , and baseline methods .

4.1 SETUP

Datasets. We select three primary domains for our experiments: **general**, **code**, and **mathematics**. For the general domain, we use the **MMLU** benchmark(Hendrycks et al., 2021), which tests the model's world knowledge and problem-solving skills across diverse subjects. In the code domain, we leverage the **MBPP**(Austin et al., 2021) and **HumanEval** datasets(Chen et al., 2021) to assess coding capabilities, including language comprehension and algorithmic reasoning. For the mathematics domain, we utilize **GSM8K**(Cobbe et al., 2021) and **MathQA**(Amini et al., 2019), which consist of elementary-level mathematical problems covering topics such as algebra and probability. We use the validation sets from **MMLU**, **MBPP**, **MathQA**, and **GSM8K** as reference data for DOWP, with final evaluations conducted on their respective test sets. For **HumanEval**, the MBPP validation set is used as reference data for DOWP, while the evaluation is performed on the full HumanEval dataset. In terms of evaluation setup, we use a **5-shot** approach to assess model performance on the **MMLU** dataset, where the model was provided with five example questions and answers before making predictions. For the other datasets (**MBPP**, **HumanEval**, **GSM8K**, and **MathQA**), we conduct evaluations in a **0-shot** setting.

Baseline & Foundation Models. Our experiments utilize four baseline models: **LLaMA-2-7b-chat**, **LLaMA-2-13b-chat**, **Gemma-7b**, and **Gemma-2-9b**. The **LLaMA-2** series and **Gemma** models, based on transformer architecture, are designed for dialogue and natural language understanding tasks. The **7b**, **13b**, and **9b** variants reflect different parameter sizes, balancing computational efficiency with task complexity. Each model consists of stacked layers of **MLP** and **Self-Attention** mechanisms, which are essential for capturing long-range dependencies and processing complex token relationships, making them effective across a range of natural language processing tasks.

Evaluation Metrics. We use **accuracy** (*acc*% ↑) as the primary evaluation metric across tasks, defined as the ratio of correctly answered questions to the total number of questions. For **mathematics** and **general** tasks, accuracy is the sole metric for assessing performance. For coding tasks, we evaluate model performance using **pass@1** and **pass@10**.

The **pass@k(↑)** metric allows the model to generate k different solutions for a given problem and measures the probability that at least one of these k solutions is correct. This is calculated as:

$$\textbf{pass@k} = 1 - \prod_{i=1}^{n} (1 - P_i) \,, \tag{11}$$

where P_i is the probability that the model's i-th solution is correct, and k is the number of trials.

4.2 MAIN RESULTS.

DOWP. We apply the DOWP algorithm to selected pre-trained language models to assess the effectiveness of DOWP in enhancing task-specific accuracy across a range of benchmark datasets. **Firstly,** the application of DOWP results in consistent performance improvements with an ***average gain of 2.04%*** over the baseline models, as shown in Table 1. Specifically, LLaMA-2-7b-chat's accuracy on MMLU increases by 1.98%, while its performance on MBPP (pass@1) rose by 2.08%, and its accuracy on GSM8K improves by 1.97%. Similar patterns are observed for the other models.

Notably, Gemma-7b exhibits an increase of 3.26% in MBPP (pass@10) and a 2.4% improvement in MathQA accuracy, demonstrating DOWP's efficacy across different models and tasks. **Secondly,** as shown in Figure 5, the performance generally lies within ***the improvement range of 2% to 3%*** across tasks, with the highest reaching up to 6.8%. These gains underscore both the algorithm's effectiveness and the stability of its enhancements. The results suggest that DOWP enhances large-scale models by improving accuracy and maintaining stability. Its ability to purify domain-specific weights ensures efficient operation across diverse datasets and architectures.

Table 1: Performance comparison of DOWP and FREE-MOE with baseline on foundation models.

	Method	MMLU	MBPP		HumanEval		GSM8K	MathQA
		acc	pass@1	pass@10	pass@1	pass@10	acc	acc
LLaMA-2-7b-chat	BASELINE	45.81	19.24	23.60	14.45	19.51	20.24	25.33
	DOWP	47.79	21.32	26.40	15.73	20.73	22.21	27.34
	Improvement	+1.98	+2.08	+2.80	+1.28	+1.22	+1.97	+2.01
	FREE-MOE	47.34	20.58	25.80	14.51	19.51	20.79	26.13
	Improvement	+1.53	+1.34	+2.20	+0.06	±0	+0.55	+0.80
LLaMA-2-13b-chat	BASELINE	52.34	9.68	13.00	18.66	28.05	31.77	24.86
	DOWP	53.18	11.52	16.00	19.45	29.88	34.42	27.57
	Improvement	+0.84	+1.84	+3.00	+0.79	+1.83	+2.65	+2.71
	FREE-MOE	52.93	12.39	14.80	19.13	29.27	33.86	26.34
	Improvement	+0.59	+2.71	+1.80	+0.47	+1.22	+2.09	+1.48
Gemma-7b	BASELINE	63.56	2.94	9.00	15.31	20.12	57.92	37.12
	DOWP	65.30	6.20	15.80	16.77	22.56	59.59	39.57
	Improvement	+1.74	+3.26	+6.80	+1.46	+2.44	+1.67	+2.45
	FREE-MOE	65.05	5.85	13.90	12.93	18.29	59.29	38.79
	Improvement	+1.49	+2.91	+4.90	−2.38	−1.83	+1.37	+1.67
Gemma-2-9b	BASELINE	69.71	8.36	9.80	12.87	18.90	68.46	50.75
	DOWP	71.07	8.52	10.80	15.12	22.56	69.98	51.22
	Improvement	+1.36	+0.16	+1.00	+2.25	+3.66	+1.52	+0.47
	FREE-MOE	70.90	8.28	10.40	14.33	20.73	69.45	50.97
	Improvement	+1.19	−0.08	+0.60	+1.46	+1.83	+0.99	+0.22

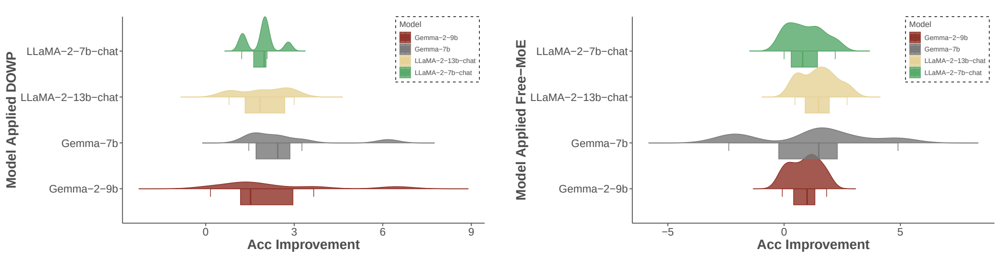

Figure 5: Accuracy improvement comparison of models using DOWP and Free-MoE methods across various architectures.

FREE-MOE. To make further comparison, we evaluate the FREE-MOE architecture on the same set of LLMs to examine its effectiveness. **Firstly,** applying FREE-MOE also led to noticeable performance gains of 1.11% in average, though the improvements were generally more moderate compared to DOWP, as shown in Table 1. In detail, LLaMA-2-7b-chat's accuracy on MMLU increases by 1.53%, while its performance on MBPP (pass@1) improves by 1.34%, and its accuracy on GSM8K see a 0.55% rise. Similarly, Gemma-7b's performance in MBPP (pass@10) increases by 2.91%, with MathQA showing a 1.67% gain. These results demonstrate that employing FREE-MOE yields consistent improvements. **Secondly,** the accuracy improvements under FREE-MOE primarily fall within the range of 0.5% to 2.5%, with the highest to 4.9%, as shown in Figure 5.

The results suggest that FREE-MOE, while less impactful than DOWP in terms of absolute gains, offers a viable and stable method for enhancing model performance with minimal additional computation. Its tuning-free nature make it particularly useful for models that need to balance task specificity, suggesting that FREE-MOE could be highly beneficial in scenarios where computational resources are limited, but consistent improvements across a wide range of tasks is still required.

4.3 Ablation Studies

In the ablation studies, we use the LLaMA-2-7b-chat model due to its stable performance in previous results. Employing DOWP, we analyze purification ratios, layers, and patch-square configurations. Furthermore, employing FREE-MOE, we analyze the k-means clustering process.

Purification Ratio. We purify the all model layers (layers 0 to 31) using a 1×1 patch-square configuration and examine different ratios on the MMLU dataset categorized into 12 groups. With a **5% purification ratio**, accuracy reaches 47.79%, a 1.98% increase over the 45.81% achieves with a 3% ratio. This demonstrates the 5% ratio effectively balances accuracy and computational cost, as shown in Table 2.

Table 2: DOWP Performance of Different Purification Ratio on MMLU Dataset.

	Ratio	MMLU(%)
Accuracy	base	45.81
	1%	47.75
	3%	47.85
	5%	47.79

Purification Sublayers. We then apply a 5% purification to MLP layers and Self-Attention layers, from layers 0 to 31, evaluating the impact on the GSM8K and MathQA, divided into 8 categories. Results shows purifying the Self-Attention layers yields the best on GSM8K, with a 3.18% improvement. On MathQA, the combination performs best, reaching a 2.01% increase, as shown in Table 3.

Table 3: DOWP Performance of Purifying Different Sublayers on GSM8K and MathQA Datasets.

	Patch	Datasets	
		GSM8K(%)	MathQA(%)
Accuracy	base	20.24	25.33
	MLP	21.61	26.87
	Self-Attention	23.42	25.90
	Combination	22.21	27.34

Patch-square Configuration. Besides, based on 5% purification ratio, we evaluate different patch-square configurations on the MBPP and HumanEval, divided into 3 categories. For MBPP, the 1×1 **patch-square** achieves the best performance on pass@1 with a 1.56% improvement, and on pass@10 with a 2.40% increase. Similarly, on HumanEval, the 1×1 configuration lead with 1.28% gains for pass@1 and 1.22% for pass@10 respectively over the baseline, as shown in Table 4.

Table 4: DOWP Performance of Different Patch Size on MBPP and HumanEval Datasets.

	Patch	MBPP(%)		HumanEval(%)	
		@1	@10	@1	@10
pass@k	base	19.24	23.60	14.45	19.51
	1×1	20.80	26.00	15.73	20.73
	2×2	19.88	25.60	15.67	20.12
	4×4	18.58	24.00	14.88	20.73
	16×16	18.40	24.40	13.97	17.68

K-means Clustering. Finally, we examine the impact of different K values applied in FREE-MOE in the K-means clustering step on the MMLU dataset, divided into 12 categories. We vary the number of clusters from 8 to 16, the results show that with **K=12**, the accuracy reaches the highest value of 47.79%, outperforming other cluster settings, as shown in Table 5.

Table 5: FREE-MOE Performance of Different K-means on MMLU Dataset.

	K	MMLU(%)
Accuracy	10	47.46
	12	47.79
	14	47.27

5 Conclusion

In this work, we introduced FREE-MOE, a novel framework designed to address tuning-related challenges in the MoE architecture. Specifically, We proposed the DOWP Alg. and incorporated a trainable router to dynamically activate domain-specific subnetworks. FREE-MOE achieves 1) tuning-free, 2) highly portable, and 3) parameter efficiency, and can integrate into any transformer-based LLM without model-specific adjustments. The experiments demonstrated consistent performance improvements, validating FREE-MOE's capability to optimize task-specific responses and its potential for wide application in pre-trained LLMs. Our method thus presents a promising solution for enhancing large model scalability and adaptability.

References

Aida Amini, Saadia Gabriel, Peter Lin, Rik Koncel-Kedziorski, Yejin Choi, and Hannaneh Hajishirzi. Mathqa: Towards interpretable math word problem solving with operation-based formalisms, 2019. URL https://arxiv.org/abs/1905.13319.

Anthropic. Towards monosemanticity: Decomposing language models with dictionary learning, 2023. URL https://transformer-circuits.pub/2023/monosemantic-features/index.html. Accessed: 2024-09-07.

Jacob Austin, Augustus Odena, Maxwell Nye, Maarten Bosma, Henryk Michalewski, David Dohan, Ellen Jiang, Carrie Cai, Michael Terry, Quoc Le, and Charles Sutton. Program synthesis with large language models, 2021. URL https://arxiv.org/abs/2108.07732.

Trenton Bricken, Adly Templeton, Joshua Batson, Brian Chen, Adam Jermyn, Tom Conerly, Nick Turner, Cem Anil, Carson Denison, Amanda Askell, et al. Towards monosemanticity: Decomposing language models with dictionary learning. *Transformer Circuits Thread*, 2, 2023.

K. Chen, L. Xu, and H. Chi. Improved learning algorithms for mixture of experts in multiclass classification. *Neural Networks*, 12(9):1229–1252, 1999.

Mark Chen, Jerry Tworek, Heewoo Jun, Qiming Yuan, Henrique Ponde de Oliveira Pinto, Jared Kaplan, Harri Edwards, Yuri Burda, Nicholas Joseph, Greg Brockman, Alex Ray, Raul Puri, Gretchen Krueger, Michael Petrov, Heidy Khlaaf, Girish Sastry, Pamela Mishkin, Brooke Chan, Scott Gray, Nick Ryder, Mikhail Pavlov, Alethea Power, Lukasz Kaiser, Mohammad Bavarian, Clemens Winter, Philippe Tillet, Felipe Petroski Such, Dave Cummings, Matthias Plappert, Fotios Chantzis, Elizabeth Barnes, Ariel Herbert-Voss, William Hebgen Guss, Alex Nichol, Alex Paino, Nikolas Tezak, Jie Tang, Igor Babuschkin, Suchir Balaji, Shantanu Jain, William Saunders, Christopher Hesse, Andrew N. Carr, Jan Leike, Josh Achiam, Vedant Misra, Evan Morikawa, Alec Radford, Matthew Knight, Miles Brundage, Mira Murati, Katie Mayer, Peter Welinder, Bob McGrew, Dario Amodei, Sam McCandlish, Ilya Sutskever, and Wojciech Zaremba. Evaluating large language models trained on code, 2021. URL https://arxiv.org/abs/2107.03374.

Karl Cobbe, Vineet Kosaraju, Mohammad Bavarian, Mark Chen, Heewoo Jun, Lukasz Kaiser, Matthias Plappert, Jerry Tworek, Jacob Hilton, Reiichiro Nakano, Christopher Hesse, and John Schulman. Training verifiers to solve math word problems, 2021. URL https://arxiv.org/abs/2110.14168.

Ronan Collobert, Samy Bengio, and Yoshua Bengio. A parallel mixture of svms for very large scale problems. *Neural Computation*, 14:1105–1114, 2002.

Dheeru Dua, Shruti Bhosale, Vedanuj Goswami, James Cross, Mike Lewis, and Angela Fan. Tricks for training sparse translation models. In Marine Carpuat, Marie-Catherine de Marneffe, and Ivan Vladimir Meza Ruiz (eds.), *Proceedings of the 2022 Conference of the North American Chapter of the Association for Computational Linguistics: Human Language Technologies*, pp. 3340–3345, July 2022.

Nelson Elhage, Neel Nanda, Catherine Olsson, Tom Henighan, Nicholas Joseph, Ben Mann, Amanda Askell, Yuntao Bai, Anna Chen, Tom Conerly, et al. A mathematical framework for transformer circuits. *Transformer Circuits Thread*, 1(1):12, 2021.

William Fedus, Barret Zoph, and Noam Shazeer. Switch transformers: Scaling to trillion parameter models with simple and efficient sparsity. *Journal of Machine Learning Research*, 23(120):1–39, 2022.

Suchin Gururangan, Mike Lewis, Ari Holtzman, Noah A. Smith, and Luke Zettlemoyer. DEMix layers: Disentangling domains for modular language modeling. In Marine Carpuat, Marie-Catherine de Marneffe, and Ivan Vladimir Meza Ruiz (eds.), *Proceedings of the 2022 Conference of the North American Chapter of the Association for Computational Linguistics: Human Language Technologies*, Seattle, United States, July 2022. Association for Computational Linguistics.

Song Han, Jeff Pool, John Tran, and William J. Dally. Learning both weights and connections for efficient neural networks, 2015. URL https://arxiv.org/abs/1506.02626.

Dan Hendrycks, Collin Burns, Steven Basart, Andy Zou, Mantas Mazeika, Dawn Song, and Jacob Steinhardt. Measuring massive multitask language understanding, 2021. URL https://arxiv.org/abs/2009.03300.

Robert A Jacobs, Michael I Jordan, Steven J Nowlan, and Geoffrey E Hinton. Adaptive mixtures of local experts. *Neural computation*, 3(1):79–87, 1991.

Michael I Jordan and Robert A Jacobs. Hierarchical mixtures of experts and the em algorithm. *Neural computation*, 6(2):181–214, 1994.

Jared Kaplan, Sam McCandlish, Tom Henighan, Tom B Brown, Benjamin Chess, Rewon Child, Scott Gray, Alec Radford, Jeffrey Wu, and Dario Amodei. Scaling laws for neural language models. *arXiv preprint arXiv:2001.08361*, 2020.

Sneha Kudugunta, Yanping Huang, Ankur Bapna, Maxim Krikun, Dmitry Lepikhin, Minh-Thang Luong, and Orhan Firat. Beyond distillation: Task-level mixture-of-experts for efficient inference, 2021. URL https://arxiv.org/abs/2110.03742.

Dmitry Lepikhin, HyoukJoong Lee, Yuanzhong Xu, Dehao Chen, Orhan Firat, Yanping Huang, Maxim Krikun, Noam Shazeer, and Zhifeng Chen. Gshard: Scaling giant models with conditional computation and automatic sharding. In *International Conference on Learning Representations*, 2020.

Jianxin Ma, Zhe Zhao, Xiao Yi, Jilin Chen, Lichan Hong, and Ed H Chi. Modeling task relationships in multi-task learning with multi-gate mixture-of-experts. In *Proceedings of the 24th ACM SIGKDD International Conference on Knowledge Discovery & Data Mining*, pp. 1930–1939, 2018.

Chris Olah, Nick Cammarata, Chelsea Voss, Ludwig Schubert, and Gabriel Goh. Naturally occurring equivariance in neural networks. *Distill*, 5(12):e00024–004, 2020.

David Patterson, Joseph Gonzalez, Quoc Le, Chen Liang, Lucia Munguia, David Rothchild, and Jeffrey Dean. Carbon emissions and large neural network training. *arXiv preprint arXiv:2104.10350*, 2021.

Michael Petrov, Chelsea Voss, Ludwig Schubert, Nick Cammarata, Gabriel Goh, and Chris Olah. Weight banding. *Distill*, 6(4):e00024–009, 2021.

Carl Rasmussen and Zoubin Ghahramani. Infinite mixtures of gaussian process experts. In *Advances in neural information processing systems*, volume 14, 2001.

Xiaozhe Ren, Pingyi Zhou, Xinfan Meng, Xinjing Huang, Yadao Wang, Weichao Wang, Pengfei Li, Xiaoda Zhang, Alexander Podolskiy, Grigory Arshinov, Andrey Bout, Irina Piontkovskaya, Jiansheng Wei, Xin Jiang, Teng Su, Qun Liu, and Jun Yao. Pangu-Σ: Towards trillion parameter language model with sparse heterogeneous computing, 2023. URL https://arxiv.org/abs/2303.10845.

Carlos Riquelme, Joan Puigcerver, Basil Mustafa, Mario Neumann, Rodolphe Jenatton, Adrià Susano Pinto, Daniel Keysers, and Neil Houlsby. Scaling vision with sparse mixture of experts. In *Advances in Neural Information Processing Systems*, volume 34, pp. 8583–8595, 2021.

Stephen Roller, Sainbayar Sukhbaatar, Arthur Szlam, and Jason E Weston. Hash layers for large sparse models. In A. Beygelzimer, Y. Dauphin, P. Liang, and J. Wortman Vaughan (eds.), *Advances in Neural Information Processing Systems*, 2021. URL https://openreview.net/forum?id=lMgDDWb1ULW.

Noam Shazeer, Azalia Mirhoseini, Krzysztof Maziarz, Andy Davis, Quoc V. Le, Geoffrey E. Hinton, and Jeff Dean. Outrageously large neural networks: The sparsely-gated mixture-of-experts layer. In *International Conference on Learning Representations*, 2017.

Emma Strubell, Ananya Ganesh, and Andrew McCallum. Energy and policy considerations for deep learning in nlp. In *Proceedings of the 57th Annual Meeting of the Association for Computational Linguistics*, pp. 3645–3650. Association for Computational Linguistics, 2019. doi: 10.18653/v1/P19-1355. URL https://doi.org/10.18653/v1/P19-1355.

Volker Tresp. A bayesian committee machine. *Neural Computation*, 12(11):2719–2741, 2000.

Chelsea Voss, Gabriel Goh, Nick Cammarata, Michael Petrov, Ludwig Schubert, and Chris Olah. Branch specialization. *Distill*, 6(4):e00024–008, 2021.

Lemeng Wu, Mengchen Liu, Yinpeng Chen, Dongdong Chen, Xiyang Dai, and Lu Yuan. Residual mixture of experts, 2022. URL https://arxiv.org/abs/2204.09636.

Yanqi Zhou, Tao Lei, Hanxiao Liu, Nan Du, Yanping Huang, Vincent Y. Zhao, Andrew M. Dai, Zhifeng Chen, Quoc V. Le, and James Laudon. Mixture-of-experts with expert choice routing. In Alice H. Oh, Alekh Agarwal, Danielle Belgrave, and Kyunghyun Cho (eds.), *Advances in Neural Information Processing Systems*, 2022. URL https://openreview.net/forum?id=jdJo1HIVinI.

Barret Zoph, Irwan Bello, Sameer Kumar, Nan Du, Yanping Huang, Jeff Dean, Noam Shazeer, and William Fedus. St-moe: Designing stable and transferable sparse expert models, 2022. URL https://arxiv.org/abs/2202.08906.

Simiao Zuo, Xiaodong Liu, Jian Jiao, Young Jin Kim, Hany Hassan, Ruofei Zhang, Jianfeng Gao, and Tuo Zhao. Taming sparsely activated transformer with stochastic experts. In *ICLR*, 2022. URL http://dblp.uni-trier.de/db/conf/iclr/iclr2022.html#Zuo00KHZGZ22.

A Scaling Hidden Layers into Patches Maintains Information in Self-Attention and MLP

In Transformer models, the Self-Attention and MLP layers are critical for capturing global contextual information and performing non-linear transformations on feature representations. The scaling of hidden layers into patches might raise concerns about the potential loss of information, but this process is designed to preserve both local and global relationships in the model.

Global Context Preservation in Self-Attention. The Self-Attention mechanism ensures that every token in the input sequence can attend to all other tokens, capturing global dependencies. This operation is described by:

$$\text{Attention}(Q, K, V) = \text{softmax}\left(\frac{QK^T}{\sqrt{d_k}}\right)V \tag{12}$$

Where: Q, K, and V are the Query, Key, and Value matrices. d_k is the dimensionality of the Key vectors. By scaling hidden layers into patches, each patch retains local interactions within the patch. Meanwhile, the Self-Attention mechanism ensures that global interactions between patches are maintained. This is because the attention mechanism operates across all patches, allowing the model to propagate global information and maintain context across the entire sequence of patches. As a result, the scaled matrix retains the full global context, ensuring no information is lost during patch scaling.

Patch Scaling and Information Compression. When the hidden layers are scaled by a factor α, the resulting reduced matrix of size $\beta X \times \beta Y$ ($\beta = 1/\alpha$) has elements that correspond to patches in the original matrix. Each patch P_{ij} captures a compressed representation of the information within the original matrix. By aggregating the contributions from each element in a patch, the scaled matrix effectively compresses the local information, while Self-Attention ensures that this compressed representation continues to interact globally. The importance of each patch is calculated as:

$$\theta_{ij} = \sum_{(m,n)\in P_{ij}} (|W_{mn}| \times \|X_{mn}\|_2) \tag{13}$$

This compression allows for efficient representation of both local and global information, preserving the integrity of the original model.

MLP Layer and Information Flow. Following Self-Attention, the MLP layer processes the globally-contextualized output. The MLP is defined as:

$$\text{MLP}(h) = \sigma(W_2 \cdot \text{ReLU}(W_1 \cdot h)) \tag{14}$$

Where: h is the output from Self-Attention. W_1 and W_2 are the weight matrices in the MLP. σ is the activation function (typically ReLU). The MLP performs non-linear transformations on the compressed feature representations from the patches. Since the MLP does not rely on spatial relationships, it processes the patch-level information without any risk of information loss. The critical feature transformations in the MLP are unaffected by the scaling process, ensuring that the information flow remains intact.

B Procedure of DOWP to Select the Best θ

In this section, we present the procedure for selecting the optimal threshold θ in the Domain-Oriented Weight Purification (DOWP) method. The goal is to assess the impact of varying θ values on performance across multiple datasets and domains, specifically MMLU, GSM8K, MathQA, and HumanEval. Each table provides a comprehensive comparison of the DOWP performance over different ranges of θ, from 50% to 100%, highlighting its effectiveness in selecting the most relevant experts in various domains.

Table 6: Performance comparison of DOWP throughout all MMLU domains with different θ.

cluster_id	Samples	50-55%	55-60%	60-65%	65-70%	70-75%	75-80%	80-85%	85-90%	90-95%	95-100%	Max (%)	Ratio (%)
mmlu_0	2047	57.79	58.72	58.96	59.26	59.99	59.94	60.67	60.23	60.77	60.92	60.92	14.58
mmlu_1	1518	35.57	34.72	34.32	35.70	35.38	35.31	35.84	35.44	36.17	35.77	36.17	10.81
mmlu_2	895	23.02	24.02	22.57	23.35	23.02	22.01	22.46	22.68	22.79	22.57	24.02	6.37
mmlu_3	1586	48.93	47.92	49.37	48.99	49.87	49.50	49.43	50.44	50.88	51.01	51.01	11.29
mmlu_4	212	27.83	28.77	28.30	25.94	28.77	26.89	27.83	26.89	27.36	26.89	28.77	1.51
mmlu_5	1477	59.58	59.04	60.39	59.51	60.12	60.80	60.93	61.61	61.61	61.75	61.75	10.52
mmlu_6	322	35.09	32.92	33.85	34.78	33.54	34.78	33.54	34.16	35.09	35.09	35.09	2.29
mmlu_7	434	27.65	25.58	29.95	26.96	26.96	27.19	28.11	29.72	27.19	29.49	29.95	3.09
mmlu_8	2016	55.21	55.36	55.46	55.51	56.15	55.56	56.35	57.04	57.19	57.44	57.44	14.36
mmlu_9	1839	46.66	47.53	46.82	46.49	47.36	47.74	47.36	48.02	48.45	48.29	48.45	13.09
mmlu_10	1174	30.92	30.15	31.26	31.09	30.49	30.15	30.83	32.03	32.28	31.86	32.28	8.36
mmlu_11	522	42.34	45.21	44.25	42.91	46.74	45.40	46.74	47.32	46.36	47.13	47.32	3.72

Table 7: Performance comparison of DOWP throughout all GSM8K domains with different θ.

cluster_id	Samples	50-55%	55-60%	60-65%	65-70%	70-75%	75-80%	80-85%	85-90%	90-95%	95-100%	Max (%)	Ratio (%)
gsm8k_0	240	12.92	15.00	15.83	18.75	13.75	17.08	16.67	17.50	15.83	16.67	18.75	18.20
gsm8k_1	8	0.00	12.50	12.50	37.50	25.00	12.50	12.50	37.50	0.00	12.50	37.50	0.61
gsm8k_2	225	17.78	21.78	18.22	24.00	22.67	22.67	22.22	21.78	20.44	24.00	24.00	17.06
gsm8k_3	361	18.28	16.90	19.67	20.50	19.94	23.82	21.05	23.82	21.61	23.82	23.82	27.37
gsm8k_4	113	13.27	17.70	9.73	15.04	15.93	19.47	17.70	13.27	17.70	16.81	19.47	8.57
gsm8k_5	193	12.44	10.88	12.95	13.99	15.03	17.62	20.73	18.65	17.10	19.69	20.73	14.63
gsm8k_6	6	33.33	16.67	50.00	33.33	33.33	16.67	33.33	33.33	16.67	50.00	50.00	0.45
gsm8k_7	173	16.18	14.45	17.92	23.12	17.34	19.08	17.34	19.65	18.50	19.65	23.12	13.12

Table 8: Performance comparison of DOWP throughout all MathQA domains with different θ.

cluster_id	Samples	50-55%	55-60%	60-65%	65-70%	70-75%	75-80%	80-85%	85-90%	90-95%	95-100%	Max (%)	Ratio (%)
mathqa_0	289	19.03	19.72	20.42	23.53	26.99	28.72	26.30	22.84	26.30	22.15	28.72	9.68
mathqa_1	318	24.53	24.84	24.21	22.96	31.45	23.58	29.87	29.25	26.42	25.79	31.45	10.65
mathqa_2	453	20.75	22.30	27.15	22.96	24.06	25.39	23.18	26.49	25.39	22.96	27.15	15.18
mathqa_3	107	24.30	27.10	28.97	20.56	28.04	27.10	28.04	20.56	22.43	20.56	28.97	3.58
mathqa_4	238	24.37	20.17	29.83	21.01	22.69	29.41	22.69	27.31	29.41	28.15	29.83	7.97
mathqa_5	269	26.77	20.45	24.91	25.65	29.37	27.14	25.65	21.56	23.79	29.00	29.37	9.01
mathqa_6	659	24.28	19.58	20.49	21.40	20.64	22.91	21.55	18.97	20.64	19.88	24.28	22.08
mathqa_7	652	20.09	21.47	21.32	24.08	22.70	22.70	25.92	24.54	23.47	22.55	25.92	21.84

Table 9: Performance comparison of DOWP throughout all HumanEval domains with different θ.

cluster_id	Metric	Samples	50-55%	55-60%	60-65%	65-70%	70-75%	75-80%	80-85%	85-90%	90-95%	95-100%	Max (%)	Ratio (%)
humaneval_0	pass@1	44	11.82	17.05	15.68	14.77	15.00	16.36	17.05	15.23	15.45	14.77	17.05	26.83
humaneval_1	pass@1	75	8.27	9.47	10.80	10.67	13.07	15.33	12.67	13.20	13.47	13.33	15.33	45.73
humaneval_2	pass@1	45	6.89	12.22	11.11	9.33	14.22	14.00	15.11	14.00	14.89	15.11	15.11	27.44
humaneval_0	pass@10	44	18.18	25.00	25.00	18.18	22.73	18.18	25.00	18.18	20.45	20.45	25.00	26.83
humaneval_1	pass@10	75	10.67	14.67	13.33	12.00	18.67	18.67	16.00	17.33	17.33	16.00	18.67	45.73
humaneval_2	pass@10	45	8.89	15.56	15.56	13.33	15.56	15.56	17.78	15.56	20.00	17.78	20.00	27.44

Table 10: Performance comparison of DOWP throughout all MBPP domains with different θ.

cluster_id	Metric	Samples	50-55%	55-60%	60-65%	65-70%	70-75%	75-80%	80-85%	85-90%	90-95%	95-100%	Max (%)	Ratio (%)
mbpp_0	pass@1	185	35.68	34.32	33.89	38.16	34.05	35.19	37.51	34.65	36.65	36.38	38.16	37.00
mbpp_1	pass@1	53	17.74	15.47	20.19	27.92	22.83	25.47	23.96	20.75	19.62	22.08	27.92	10.60
mbpp_2	pass@1	262	7.29	6.18	5.84	6.34	6.56	8.09	6.56	6.45	7.75	7.52	8.09	52.40
mbpp_0	pass@10	185	40.54	43.24	42.16	42.16	40.54	41.08	44.32	39.46	42.70	42.16	44.32	37.00
mbpp_1	pass@10	53	24.53	26.42	28.30	32.08	28.30	35.85	30.19	26.42	26.42	33.96	35.85	10.60
mbpp_2	pass@10	262	9.16	9.16	9.92	9.16	10.31	11.83	9.92	10.31	11.83	11.45	11.83	52.40

C Threshold-Based Performance Analysis Across Datasets

This appendix provides a comprehensive analysis of the performance trends observed across varying threshold θ values for the datasets GSM8K, MathQA, HumanEval, MBPP, and MMLU. Each dataset, representing a distinct domain such as mathematics, programming, and general knowledge, showcases unique response patterns when applying the FREE-MOE framework. As θ increases, we observe noticeable fluctuations in accuracy, highlighting the dynamic behavior of domain-specific subnetworks. The results consistently demonstrate that activating experts based on purified domain-specific weights yields stable improvements across tasks, while maintaining computational efficiency. This analysis reinforces the scalability and adaptability of FREE-MOE, validating its ability to enhance task-specific accuracy without the need for fine-tuning.

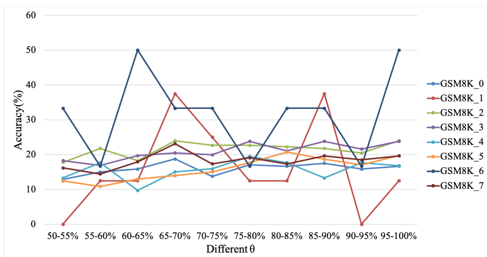

(a) GSM8K

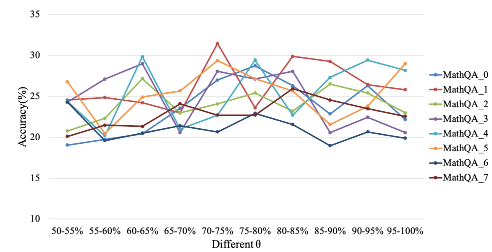

(b) MathQA

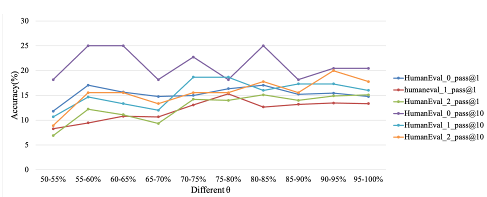

(c) HumanEval

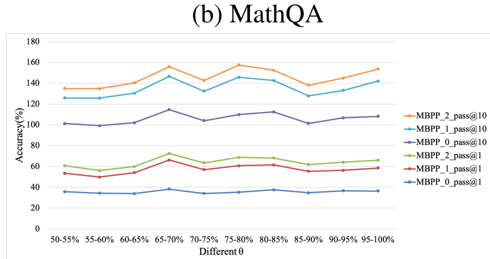

(d) MBPP

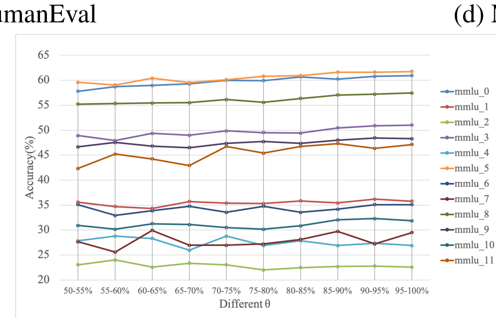

(e) MMLU

Figure 6: Accuracy comparison of DOWP across different thresholds θ for various datasets including GSM8K, MathQA, HumanEval, MBPP, and MMLU. Each subfigure (a-e) shows performance variations with respect to the θ values, highlighting dataset-specific accuracy trends.